Journal of Materials Chemistry A

Accepted Manuscript

This article can be cited before page numbers have been issued, to do this please use: H. Jia, Y. Yao, J. Zhao, Y. Gao, Z. Luo and P. Du, *J. Mater. Chem. A*, 2017, DOI: 10.1039/C7TA07978H.

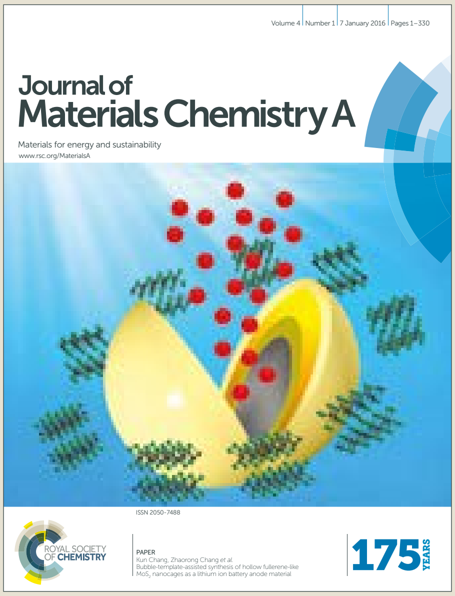

View Article Online
DOI: 10.1039/C7TA07978H

Novel Two-Dimensional Nickel Phthalocyanine-Based Metal-Organic Framework for Highly Efficient Water Oxidation Catalysis

Hongxing Jia,[a] *Yuchuan Yao,*[a] *Jiangtao Zhao,*[b] *Yuyue Gao,*[a] *Zhenlin Luo,*[b] *Pingwu Du**[a]

[a] Hefei National Laboratory for Physical Sciences at Microscale, CAS Key Laboratory of Materials for Energy Conversion, Department of Materials Science and Engineering, *i*ChEM (Collaborative Innovation Center of Chemistry for Energy Materials), University of Science and Technology of China (USTC), 96 Jinzhai Road, Hefei, Anhui Province, 230026, P. R. China.

[b] National Synchrotron Radiation Laboratory, University of Science and Technology of China (USTC), 96 Jinzhai Road, Hefei, Anhui Province, 230026, P.R.China.

*E-mail: dupingwu@ustc.edu.cn

View Article Online
DOI: 10.1039/C7TA07978H

Abstract. Large π-conjugated conductive two-dimensional (2D) metal-organic frameworks (MOFs) *via* bottom-up approach have recently emerged as a novel and interesting 2D material. For the first time, herein we demonstrate the design and successful bottom-up fabrication of a novel noble-metal-free nickel phthalocyanine-based 2D MOF (NiPc-MOF) for highly efficient water oxidation catalysis. This NiPc-MOF can be easily grown on various substrates. The thin film deposited on FTO showed high catalytic oxygen evolution reaction (OER) activity with a very low onset potential (< 1.48 V, overpotential < 0.25 V), high mass activity (883.3 A g^{-1}), and excellent catalytic durability. To the best of our knowledge, this present 2D MOF film catalyst represents the best OER catalytic activity among molecular catalyst-based materials reported so far. This work represents the first synthesis of nickel phthalocyanine-based 2D MOF material and the application of π-conjugated 2D MOF for water oxidation.

Keywords: Molecular catalyst; Water oxidation; Oxygen evolution reaction; Noble-metal-free catalyst; Two-dimensional materials

View Article Online
DOI: 10.1039/C7TA07978H

1. Introduction

Owing to their unique physical and chemical properties, two-dimensional (2D) materials have attracted much attention in the past decade, including research on graphene,[1, 2] graphdiyne,[3] metal chalcogenides,[4, 5] metal oxides,[6] and metal hydroxides.[7] These materials have been investigated for many applications in sensors,[8] photonics,[9] catalysis,[10] and optoelectronics.[9] So far, most 2D materials have been synthesized through various top-down exfoliation strategies from bulk-layered crystalline materials.[4] However, the harsh conditions in the top-down approach could make the exfoliation processes difficult and expensive. In addition, the properties of 2D nanosheets are limited by their bulk precursors and it is difficult to produce 2D materials with high structural or functional tunability using the top-down method.

On the other hand, the bottom-up synthetic approach can precisely control the topological molecular architecture and has emerged as a desirable method to prepare 2D molecular materials.[11, 12] Using this method, a variety of organic building blocks can be assembled into organic 2D materials under mild reaction conditions. Typical examples include covalent organic frameworks (COFs)[13, 14] and 2D metal-organic frameworks (MOFs).[12, 15, 16] COFs/MOFs are organic/coordination porous materials with extended skeletons, which show promising capacity for electrocatalysis because of their high specific surface areas and tunable porous structures.[17] However, due to their poor conductive/electric properties, very few COFs and MOFs can be directly used as highly active electrocatalysts.[18, 19] Pyrolysis of these COFs and MOFs materials or incorporating them onto carbon materials are the most commonly used methods to enhance their conductivity,[20] which may introduce complicated processes or sizable damage to their original chemical structures as well as chemical properties. In recent years, significant progress has been made in the development of π-conjugated 2D MOFs with high intrinsic electrical conductivity, some of which have been utilized as catalysts for hydrogen evolution reaction (HER)[15] and oxygen reduction reaction

View Article Online
DOI: 10.1039/C7TA07978H

(ORR).[21] To date, most reported π-conjugated 2D MOFs are fabricated from only benzene- or triphenylene-based fragments,[22, 23] and no π-conjugated 2D MOFs material has been investigated to catalyze oxygen evolution reaction (OER).

In this present study, we report the first synthesis of a novel nickel phthalocyanine-based 2D MOF (NiPc-MOF) with a formula of $[Ni_3(C_{32}H_{16}N_{16})]_n$. In the literature, no π-conjugated 2D MOFs material using phthalocyanine building block has been previously reported. The NiPc motif acts not only as the connecting unit but also as an electrocatalytically active site for catalysis. Besides the synthesis and physical characterization of the NiPc-MOF, we further explored its outstanding performance toward OER.

2. Results and discussion

2.1 Synthesis and characterization of NiPc-MOF. Figure 1 shows the synthesis and chemical structure of the NiPc-MOF material. The building block 2,3,9,10,16,17,23,24-*octa*-amino-phthalocyaninato nickel(II) ($NiPc-NH_2$) was prepared following a modified procedure[24] and confirmed by ^1H NMR spectroscopy (Figure S1), mass spectrometry (Figure S2), UV-vis absorption feature (experimental methods), and elemental analysis. The as-prepared $NiPc-NH_2$ was then reacted with nickel(II) salt ($NiCl_2·6H_2O$) in DMSO in the presence of ammonia at 60 °C for 12 hours. Subsequently, the $NiPc-NH_2$ monomers were connected with each other *via* the $Ni(isq)_2$ linker (bis(*o*-diiminobenzosemiquinonate) nickel(II), which is known for its neutral, planar, diradical structure). Finally, a huge π-conjugated 2D MOF with four-fold symmetry was formed, yielding a bulk black powder. Interestingly, the NiPc-MOF material can also be grown on a variety of supports, such as fluorine-doped tin oxide (FTO), indium tin oxide (ITO), quartz glass, and silicon wafer, resulting in a blue-black thin film under such reaction conditions.

To confirm the successful preparation of NiPc-MOF, the FT-IR spectra of NiPc-MOF and $NiPc-NH_2$ monomer were measured and the results are shown in **Figure 2**a. Both spectra show similar signals at ~1112 cm^{-1} (C-H bending mode),[25] ~1552 cm^{-1} (C=C stretching mode),[25] and ~1630 cm^{-1} (C=N stretching mode),[24] indicating that the basic building block in NiPc-MOF is similar to NiPc-NH_2. However, in contrast to NiPc-NH_2, the absence of the N-H signals (located at ~3343 cm^{-1} and ~3235 cm^{-1})[24] in NiPc-MOF suggests complete coordination between NiPc-NH_2 and nickel(II) salt to form Ni(isq)$_2$ unit. In addition, the chemical compositions of NiPc-MOF were further examined by XPS. The survey scan indicates the presence of only C, N, Ni, and O elements (Figure S3a). In the Ni 2p spectrum (Figure S3b), two sets of peaks located at 854.6 eV (Ni 2p$_{3/2}$) and 871.9 eV (Ni 2p$_{1/2}$) were observed, revealing that a single type of Ni was found in NiPc-MOF. As for the N 1s spectrum (Figure S3c), deconvolution of N 1s signals generates two peaks with binding energies of 398.8 eV (N-M) and 399.9 eV (N=C).[26] Therefore, no residual Cl^-, Ni^{2+}, or NH_4^+ ions, which are the only possible extraneous charge-balancing counterions, were detected by XPS, confirming the charge neutrality of the present NiPc-MOF material.

The morphology of bulk NiPc-MOF was probed using scanning electron microscopy (SEM) (**Figure 2**b) and transmission electron microscopy (TEM) (Figure S4). The images show homogeneous nanospheres that clumped together. Energy-dispersive X-ray (EDX) data (Figure S5) further indicate the presence of C, N, and Ni. Nitrogen adsorption measurements for bulk NiPc-MOF were performed at 77 K (Figure S6), showing a high surface area (~593 m^2 g^{-1}) by the Brunauer-Emmett-Teller (BET) method.

2.2 Crystalline structure. Powder X-ray diffraction (XRD) pattern of bulk NiPc-MOF was further measured. The result clearly demonstrates its periodic structure with intense reflection peaks at ~2.2 ° and ~4.4 °, which can be assigned to the (100) and (200) facets, respectively (**Figure 3**a-3b). These peaks indicate that the NiPc-MOF exhibits excellent long-range order within the *ab* planes. In addition, a weaker and broader peak at ~12.1 ° (corresponding to the (001) facet) can also be observed in the XRD data, suggesting relatively poor long-range stacking along the *c* direction, which has been observed in other layered materials.[15]

DOI: 10.1039/C7TA07978H

Computer simulations of crystal structures using two different stacking arrangements for NiPc-MOF material are shown in **Figure 3**c-3d. The eclipsed AA-stacking mode with P_4/mmm space group gave an XRD pattern that agrees well with the experimental result, whereas the staggered AB-stacking mode with I_4/mmm space group failed to simulate the experimental XRD peaks. As a result, the NiPc-MOF is constructed in an eclipsed AA-stacking structure with P_4/mmm space group; the unit cell parameters are $a = b = 17.9$ Å and $c = 3.3$ Å.

2.3. Electrical conductivity. In order to test the electrical properties of NiPc-MOF, thin films were grown on a quartz substrate. The scanning probe microscopy (SPM) images of NiPc-MOF film (**Figure 4**a-4b) show layered structure with a quite rough surface, and the cross-sectional analysis reveals a thickness ranging from 100 nm to 200 nm. The electrical conductivities of NiPc-MOF films on quartz were further examined using a typical four-probe method, revealing a high electrical conductivity of ~0.2 S cm^{-1} at room temperature (RT) (Figure S7), which is higher than most conductive 3D MOFs to date,[27, 28] and also comparable to some other reported 2D MOFs, such as nickel bis(dithiolene) nanosheet (two-electrode configuration, 298 K),[12] HTT-Pt network (two-probe configuration at RT),[29] and $Cu_3(HITP)_2$ (two-point-probe at RT).[30] In addition, based on the Arrhenius plot of the conductivity for NiPc-MOF (Figure S7b), the activation energy of NiPc-MOF was calculated to be 0.11 meV, which is quite small for a coordination polymer.

2.4. Characterization of NiPc-MOF film on FTO. Based on its high specific surface area, well-defined porous structure, and good conductivity, we proposed that the present NiPc-MOF material could be an excellent electrocatalyst for water oxidation catalysis. To examine the OER activity, NiPc-MOF was facilely grown on FTO substrate to give a blue-black thin film (**Figure 5**a). High coverage of the NiPc-MOF material can be clearly observed from the SEM image (**Figure 5**b) and the thickness of NiPc-MOF film on FTO was ~300 nm judged from the SPM image (Figure S8). To explore the structure of NiPc-MOF film on FTO, we scratched the film from the plate and measured the XRD data (Figure S9). The result clearly showed that the NiPc-MOF film and the NiPc-MOF powder have nearly the same XRD patterns. The catalyst loading on FTO was estimated to be ~7.6 μg cm^{-2} based on the ICP-AES results (Table S1). Electrochemical impedance spectroscopy (EIS) studies further confirm the fast ions transport dring the OER process in 1.0 M KOH (Figure S10).

2.5. OER activity of NiPc-MOF catalyst. Linear sweep voltammetry (LSV) was performed to evaluate the catalytic activity in a typical three - electrode system. The pH-dependent results revealed that the OER activity of NiPc-MOF increases with the pH values (**Figure 5**c). A plot of the potentials versus pH values at a fixed current (1.0 mA cm^{-2}) showed an almost linear relationship from pH = 7 to pH = 13.6 with a slope of -131 mV/pH unit (Figure S11). This suggests that a e^--$2H^+$ couple may be operative in our system.[31] In 1.0 M KOH, NiPc-MOF exhibited excellent activity with a sharp onset catalytic current at ~1.48 V, corresponding to a low overpotential of only 0.25 V. This onset potential of NiPc-MOF is much lower than most reported molecular OER catalysts made of noble-metal-free elements (Table S2).[32, 33] Moreover, the present NiPc-MOF catalyst even outperforms many noble metal-based OER catalysts in terms of the onset potential for OER (Table S2).[34, 35] In sharp contrast, the OER catalytic currents of the monomer NiPc-NHTs and blank FTO only start at 1.65 V and 1.80 V, respectively, which are much more positive than that of NiPc-MOF (**Figure 5**d). Impressively, NiPc-MOF showed a quite high mass activity (883.3 A g^{-1}) for OER under an overpotential of 350 mV in 1.0 M KOH, which is nearly 30-fold higher than that of RuO_2 catalyst reported in the literature.[36] To further estimate the intrinsic activity of NiPc-MOF, the turnover frequency (TOF) was calculated, giving a high value of 2.5 s^{-1}. Actually, this value is underestimated because all the nickel atoms in NiPc-MOF are assumed to be the electrochemical active sites. But even under this pessimistic assumption, the TOF value is still much higher than most reported metal-organic molecular systems (Table S2),[19, 32]

View Article Online
DOI: 10.1039/C7TA07978H

as well as many advanced inorganic materials[36, 37] under similar conditions. These results suggest that the present NiPc-MOF is an excellent and efficient catalyst for OER.

Besides the outstanding OER activity, the catalytic durability of NiPc-MOF was also examined in 1.0 M KOH. Long-term chronopotentiometry experimentation on NiPc-MOF was performed under a moderate current density of 1.0 mA cm^{-2} (**Figure 6**a). The result shows that the catalytic potential decreased slightly at the beginning and then kept almost constant at ~1.50 V for quite a long time (50 hours). The required overpotential (270 mV) is in good agreement with the LSV curves. After long-term chronopotentiometry testing, no color change could be observed in the electrolyte solution. A featureless UV-vis curve (Figure S11) was obtained, indicating that there was no leaching of soluble NiPc materials during electrolysis. In addition, the SEM image (Figure S12) and Raman spectrum (**Figure 6**b) of NiPc-MOF were further measured. The results indicate that the morphology and structure in NiPc-MOF have no significant change before and after electrochemical measurements. As for the XPS data, Ni 2p spectrum of NiPc-MOF shows a slight increase of ~0.5 eV in binding energy after OER catalysis (Figure S13), which could be attributed to Ni-O interactions in NiPc-MOF during OER, resulting in minor structural rearrangement. This observation has been also reported in other studies.[21] The minor structural rearrangement is consistent with the slight decrease of overpotential at the beginning of electrocatalysis for OER, indicating that minor structural rearrangement might be important to produce the key reaction intermediates for OER and thereafter help the enhancement of OER activity.

2.6. OER kinetics and Faradaic efficiency. To gain further insight into the OER kinetics of NiPc-MOF, Tafel analysis of electrocatalytic OER was conducted based on the corresponding LSV curve (**Figure 6**c). The NiPc-MOF exhibits a Tafel slope of 74 mV per decade in 1.0 M KOH, which is much smaller than that of many previous reported molecular OER catalysts, such as $CoH^{\beta F}CX\text{-}CO_2H$ (120 mV per decade, pH 7),[32] $Ru(bpa)(pic)_2$ derivative-MWCNTs (160 mV per decade, pH 7),[35] and Pb-TCPP catalyst (106.2 mV per dacade, pH 14),[19]

View Article Online
DOI: 10.1039/C7TA07978H

indicating its efficient electrocatalytic kinetics of OER. The oxygen evolution was confirmed by a fluorescence-based oxygen sensor during electrocatalysis under a current density of 10 mA cm^{-2} in 1.0 M KOH. The amount of oxygen was measured to be consistent with the expected value (assuming that all the charge was attributed to 4e$^-$ oxidation of H_2O), giving a high Faradaic efficiency of > 94% in 6000 seconds (**Figure 6**d).

3. Conclusions

In conclusion, an electrocatalytically active nickel phthalocyanine-based 2D metal-organic framework *via* bottom-up approach was facilely synthesized and characterized. This present study is the first on the nickel phthalocyanine unit as a key organic fragment to construct π-conjugated 2D NiPc-MOF *via* bottom-up approach. The NiPc-MOF thin film on FTO can be used as a highly active electrocatalyst for water oxidation catalysis without further pyrolysis or adding conductive materials. A series of electrochemical experiments demonstrate its outstanding OER performance under alkaline conditions, including quite low onset potential (1.48 V), high mass activity (883.3 A g^{-1}), and high TOF value (2.5 s^{-1}). In addition, the OER catalysis using NiPc-MOF shows good durability. The excellent OER performance of the present NiPc-MOF catalyst suggests the important roles of its 2D structure and good conductivity. The present study broadens the applications of π-conjugated conductive 2D MOFs materials, which may facilitate the development of this class of materials for energy applications.

4. Experimental section

Materials. *o*-phenylenediamine ($C_6H_8N_2$, 99%), tosyl chloride ($C_7H_7ClO_2S$, 99%), hydrochloric acid (HCl, 36~38%), bromine (Br_2, 99.5%), cuprous cyanide (CuCN, 99%), ammonia solution (NH_3, 25~28%), nickel(II) chloride ($NiCl_2$, 98%), 1,8-diazabicyclo[5,4,0]undec-7-ene ($C_9H_{16}N_2$, DBU, 98%), sulfuric acid (H_2SO_4, 98%), sodium

View Article Online
DOI: 10.1039/C7TA07978H

hydroxide (NaOH, 96%), nickel (II) chloride hexahydrate ($NiCl_2·6H_2O$, 98%), potassium hydroxide (KOH, 85%), dipotassium hydrogen phosphate trihydrate ($K_2HPO_4·3H_2O$, 99%), potassium dihydrogen phosphate (KH_2PO_4, 99.5%), and boric acid (H_3BO_3, 99.99%) were purchased from commercial suppliers (Alfa Aesar or Sigma Aldrich) and used without further purification. All organic solvents (pyridine, EtOH, AcOH, DMF, *n*-hexanol, CH_2Cl_2, and DMSO) were obtained from China Medicine Shanghai Chemical Reagent Co and directly used as received unless otherwise noted. All the electrolytic solutions in this contribution were freshly prepared with Millipore water (~18.0 MΩ·cm resistivity at room temperature).

Synthesis of *N,N′*-ditosyl-*o*-phenylenediamine (1), 4,5-Dibromo-*N,N′*-ditosyl-*o*-phenylenediamine (2), and 4,5-Dicyano-*N,N′*-ditosyl-*o*-phenylenediamine (3). **1**, **2**, and **3** were prepared according to the published procedures. [38-39]

Synthesis of 2,3,9,10,16,17,23,24-*octa*-tosylamido phthalocyaninato nickel(II) (NiPc-NHTs). Following a modified procedure,[38] to a suspension of **3** (933 mg, 2.0 mmol) and anhydrous $NiCl_2$ (259 mg, 2.0 mmol) in *n*-hexanol (3 mL) was added DBU (0.5 mL). The solution was heated to 160 °C under argon for 36 hours. Upon cooling to room temperature, the solvent was removed under vacuum and the resulting product was redissolved in a mixture of 5 mL acetic acid and 25 mL CH_2Cl_2. The organic extract was washed thoroughly with water, dried over anhydrous $MgSO_4$, and then evaporated to dryness. The dark green product was purified by chromatography on a silica gel column with CH_2Cl_2/MeOH (50:1) as eluent. Yield 0.33 g (34%). ^1H NMR ($CDCl_3$, 400 MHz): δ (ppm) 8.90 (s, 4H), 8.74 (s, 4H), 8.13 (s, 4H), 8.08 (d, 8H), 7.97 (s, 4H), 7.84 (d, 8H), 7.17 (d, 8H), 6.77 (d, 8H), 2.98 (s, 12H), 2.20 (s, 12H); UV-vis (CH_2Cl_2) λ_{max} (nm) 345, 637, 672.

Synthesis of 2,3,9,10,16,17,23,24-*octa*-amino-phthalocyaninato nickel(II) (NiPc-NH_2). The as-prepared NiPc-NHTs (100 mg, 52.0 μmol) was added into a mixture of 3 mL concentrated H_2SO_4 and 0.4 mL deionized water. Then the mixture was heated to 110 °C for about 1 hour. After cooling to room temperature, the reaction mixture was poured into ice-

View Article Online
DOI: 10.1039/C7TA07978H

water (20 mL). The green precipitate was collected by filtration and the solid was washed thoroughly with deionized water (20 mL×3), 10% NaOH (20 mL×3), deionized water (20 mL×3), and EtOH (20 mL×3) sequentially, giving NiPc-NH_2 as a pure black powder (30 mg, 84%). ^1H NMR (DMSO-d_6, 400 MHz): δ (ppm) 8.33 (s, 8H), 5.66 (s, 16H) (Supplementary Fig. 1); MALDI-TOF MS *m/z* = 690.1310 (M^+), calcd. for $C_{32}H_{24}N_{16}Ni^+$: 690.1723 (Supplementary Fig. 2); UV-vis (DMSO) λ_{max} (nm) 324, 505, 716; Anal. calcd. for NiPc-$NH_2 \cdot 2H_2O$ (%): C, 52.84; H, 3.88; N, 30.81. Found: C, 52.53; H, 4.01; N, 31.15.

Synthesis of NiPc-MOF. In a typical experiment, NiPc-NH_2 (30 mg, 43.4 μmol) and $NiCl_2 \cdot 6H_2O$ (21 mg, 88.4 μmol) were dissolved in 40 mL DMSO. The solution was heated to 60 °C, followed by addition of 1.0 mL concentrated aqueous ammonia in one portion. Thereafter, the resulting dark red mixture was gently stirred at this temperature for 12 hours under air. After cooling to room temperature, the resulting black powder was collected by filtration and the solid was washed thoroughly by hot DMSO (20 mL×3), deionized water (20 mL×3), MeOH (20 mL×3), and acetone (20 mL×3) sequentially, giving NiPc-MOF as a pure black powder (32 mg, 92%). To fabricate NiPc-MOF film on a supporting substrate, a quartz plate or a FTO glass plate was placed upside-up in the reaction vessel under these conditions. Then, the NiPc-MOF material can be facilely grown on the substrate, appearing as a blue-black thin film.

Characterization. ^1H NMR spectra were recorded on a Bruker AV400 instrument operating at 400 MHz. High-resolution MALDI-TOF mass spectra were measured on a Bruker Daltonics Inc. LTQ Orbitrap XL hybrid Fourier Transform High-resolution Mass Spectrometer. UV-vis spectra were collected on a UNIC-3802 spectrophotometer in standard glass cuvettes. Elemental analysis (EA) test of NiPc-NH_2 was performed on a VarioELIII elemental analyzer. Fourier transformed infrared (FT-IR) spectroscopy measurements were carried out on a Thermo Fisher Scientific instrument (Nicolet iS10). X-ray photoelectron spectroscopy (XPS) data were obtained on a Thermo ESCALAB 250 X-ray photoelectron

View Article Online
DOI: 10.1039/C7TA07978H

spectroscopy instrument using Al K_α source (15 kV, 150 W). Scanning electron microscopy (SEM) and scanning probe microscopy (SPM) images were taken with SIRION200 Schottky field emission scanning electron microscope and DI Innova scanning probe microscopy, respectively. Transmission electron microscopy (TEM) images were collected *via* a Model JEM-2011 electron microscope at an acceleration voltage of 200 kV integrated with energy-dispersive X-ray (EDX) to perform chemical analysis. Nitrogen adsorption and desorption measurements were performed on Quantachrome instrument (ASIQM0000-5) and the Brunauer-Emmett-Teller (BET) method was applied to calculate the specific surface areas. Powder X-ray diffraction (XRD) experiments for NiPc-MOF powder were implemented from 4 ° to 50 ° at the BL14B station of Shanghai Synchrotron Radiation Facility (λ = 0.68889 Å). The used X-ray photon energy is 18 keV and the diffraction patterns were recorded by a two-dimension detector (MARCCD, 3072×3072 pixels) using transmission geometry. The crystal structure analysis of NiPc-MOF film on FTO was measured by X-ray diffraction (XRD, D/max-TTR III) via graphite monochromatized Cu Kα radiation of 1.5406 Å, operated at 40 kV and 200 mA. The scanning rate was 5° min^{-1} from 3° to 40°. The electrical properties were recorded with a four-probe set-up in a Physical Property Measurement Systems (PPMS-9, Quantum Design Inc.). Elemental analyses of Ni was conducted on an Optima 7300 DV Inductively Coupled Plasma-Atomic Emission Spectrometry (ICP-AES).

XRD simulations. Two structural models of NiPc-MOF were constructed in the space groups of $P_{4/mmm}$ (eclipsed AA-stacking mode) and $I_{4/mmm}$ (staggered AB-stacking mode) using the *Materials Studio* software package. To simplify the simulations, the cell parameters of *a*, *b*, and *c* were determined based on the experimental XRD peaks. Considering the eclipsed AA-stacking mode with the space group of $P_{4/mmm}$, the experimental XRD peaks could be reproduced when the values of *a*, *b*, and *c* were set as $a = b = 17.9$ Å and $c = 3.3$ Å, while the staggered AB-stacking mode with $I_{4/mmm}$ space group failed to reproduce the experimental XRD data.

DOI: 10.1039/C7TA07978H

Electrical property measurement. Electrical conductivity data for NiPc-MOF were collected by a four-electrode set-up in a Physical Property Measurement Systems (PPMS-9, Quantum Design Inc.). NiPc-MOF film was fabricated on a quartz plate and then four parallel copper wires were fixed on the film using conductive silver adhesives. During the electrical conductivity test, the current was fixed at a constant value. The voltage drop between two inside electrodes can be recorded with the temperature change from 100 K to 400 K.

Electrochemistry. All the electrochemical experiments were conducted at room temperature on an electrochemical workstation (CHI760E, Shanghai Chen Hua Instrument Co., Ltd.) in a standard three-electrode system. The NiPc-MOF modified FTO glass was utilized as the working electrode, an Ag/AgCl electrode (3 M KCl, corrected before each experiment) as the reference electrode and a platinum wire as the counter electrode. All potentials in this contribution are quoted with respect to the reversible hydrogen electrode (RHE) based on the following equation:

$$E_{RHE} = E_{appl} + E_{Ag/AgCl} + 0.059 \times pH$$

*i*R compensation was applied in all the electrochemical measurements (80% for linear sweep voltammetry (LSV) tests). The mass activity is calculated by the following equation:

$$mass\ activity = \frac{J \times S}{m}$$

where J is the measured current density and m represents the catalyst loading amount. The turnover frequency (TOF) value is estimated according to the following equation:

$$TOF = \frac{J \times S}{4F \times n_{cat}}$$

where J is the measured current density, S is the area of the FTO electrode, F is the Faraday constant (96485 C/mol), and n_{cat} is the moles of Ni sites on the working electrode.

Supporting Information

View Article Online
DOI: 10.1039/C7TA07978H

Supporting Information is available from the Online: http://pubs.rsc.org.

Acknowledgement

This work was financially supported by the National Key Research and Development Program of China (2017YFA0402800), the National Natural Science Foundation of China (21473170, 51772285), the Fundamental Research Funds for the Central Universities (WK3430000001).

References

1. K. S. Novoselov, A. K. Geim, S. V. Morozov, D. Jiang, M. I. Katsnelson, I. V. Grigorieva, S. V. Dubonos and A. A. Firsov, *Nature*, 2005, **438**, 197-200.
2. K. S. Novoselov, A. K. Geim, S. V. Morozov, D. Jiang, Y. Zhang, S. V. Dubonos, I. V. Grigorieva and A. A. Firsov, *Science*, 2004, **306**, 666-669.
3. G. X. Li, Y. L. Li, H. B. Liu, Y. B. Guo, Y. J. Li and D. B. Zhu, *Chem. Commun.*, 2010, **46**, 3256-3258.
4. M. Chhowalla, H. S. Shin, G. Eda, L. J. Li, K. P. Loh and H. Zhang, *Nat. Chem.*, 2013, **5**, 263-275.
5. S. L. Li, K. Tsukagoshi, E. Orgiu and P. Samori, *Chem. Soc. Rev.*, 2016, **45**, 118-151.
6. N. Sakai, Y. Ebina, K. Takada and T. Sasaki, *J. Am. Chem. Soc.*, 2004, **126**, 5851-5858.
7. D. P. Yan, J. Lu, M. Wei, J. B. Han, J. Ma, F. Li, D. G. Evans and X. Duan, *Angew. Chem. Int. Ed.*, 2009, **48**, 3073-3076.
8. J. Yan, M. H. Kim, J. A. Elle, A. B. Sushkov, G. S. Jenkins, H. M. Milchberg, M. S. Fuhrer and H. D. Drew, *Nat. Nanotechnol.*, 2012, **7**, 472-478.
9. F. Bonaccorso, Z. Sun, T. Hasan and A. C. Ferrari, *Nat. Photonics*, 2010, **4**, 611-622.
10. M. Jahan, Q. L. Bao and K. P. Loh, *J. Am. Chem. Soc.*, 2012, **134**, 6707-6713.
11. X. Huang, P. Sheng, Z. Y. Tu, F. J. Zhang, J. H. Wang, H. Geng, Y. Zou, C. A. Di, Y. P. Yi, Y. M. Sun, W. Xu and D. B. Zhu, *Nat. Commun.*, 2015, **6**, 8408.

12. T. Kambe, R. Sakamoto, K. Hoshiko, K. Takada, M. Miyachi, J. H. Ryu, S. Sasaki, J. Kim, K. Nakazato, M. Takata and H. Nishihara, *J. Am. Chem. Soc.*, 2013, **135**, 2462-2465.

13. A. P. Cote, A. I. Benin, N. W. Ockwig, M. O'Keeffe, A. J. Matzger and O. M. Yaghi, *Science*, 2005, **310**, 1166-1170.

14. J. W. Colson, A. R. Woll, A. Mukherjee, M. P. Levendorf, E. L. Spitler, V. B. Shields, M. G. Spencer, J. Park and W. R. Dichtel, *Science*, 2011, **332**, 228-231.

15. A. J. Clough, J. W. Yoo, M. H. Mecklenburg and S. C. Marinescu, *J. Am. Chem. Soc.*, 2015, **137**, 118-121.

16. R. Makiura, S. Motoyama, Y. Umemura, H. Yamanaka, O. Sakata and H. Kitagawa, *Nat. Mater.*, 2010, **9**, 565-571.

17. X. Feng, X. S. Ding and D. L. Jiang, *Chem. Soc. Rev.*, 2012, **41**, 6010-6022.

18. H. B. Aiyappa, J. Thote, D. B. Shinde, R. Banerjee and S. Kurungot, *Chem. Mater.*, 2016, **28**, 4375-4379.

19. F. N. Dai, W. D. Fan, J. H. Bi, P. Jiang, D. D. Liu, X. R. Zhang, H. Lin, C. F. Gong, R. M. Wang, L. L. Zhang and D. F. Sun, *Dalton. Trans.*, 2016, **45**, 61-65.

20. L. Yang, M. G. Gao, B. Dai, X. H. Guo, Z. Y. Liu and B. H. Peng, *Electrochim. Acta*, 2016, **191**, 813-820.

21. E. M. Miner, T. Fukushima, D. Sheberla, L. Sun, Y. Surendranath and M. Dincă, *Nat. Commun.*, 2016, **7**, 10942.

22. H. Maeda, R. Sakamoto and H. Nishihara, *Langmuir*, 2016, **32**, 2527-2538.

23. L. Sun, M. G. Campbell and M. Dincă, *Angew. Chem. Int. Ed.*, 2016, **55**, 3566-3579.

24. F. Yuksel, S. Tuncel and V. Ahsen, *J. Porphyrins Phthalocyanines*, 2008, **12**, 123-130.

25. M. Samanta, U. K. Ghorai, B. Das, P. Howli, S. Das, D. Sen and K. K. Chattopadhyay, *RSC Adv.*, 2016, **6**, 42739-42744.

26. D. Sheberla, L. Sun, M. A. Blood-Forsythe, S. Er, C. R. Wade, C. K. Brozek, A. Aspuru-Guzik and M. Dincă, *J. Am. Chem. Soc.*, 2014, **136**, 8859-8862.

27. Y. Kobayashi, B. Jacobs, M. D. Allendorf and J. R. Long, *Chem. Mater.*, 2010, **22**, 4120-4122.

28. A. A. Talin, A. Centrone, A. C. Ford, M. E. Foster, V. Stavila, P. Haney, R. A. Kinney, V. Szalai, F. El Gabaly, H. P. Yoon, F. Leonard and M. D. Allendorf, *Science*, 2014, **343**, 66-69.

29. J. S. Cui and Z. T. Xu, *Chem. Commun.*, 2014, **50**, 3986-3988.

30. M. G. Campbell, D. Sheberla, S. F. Liu, T. M. Swager and M. Dincă, *Angew. Chem. Int. Ed.*, 2015, **54**, 4349-4352.

31. C. M. Che, J. Y. K. Cheng, K. K. Cheung and K. Y. Wong, *J. Chem. Soc. Dalton*, 1997, 2347-2350.

32. D. K. Dogutan, R. McGuire and D. G. Nocera, *J. Am. Chem. Soc.*, 2011, **133**, 9178-9180.

33. H. X. Jia, Z. J. Sun, D. C. Jiang and P. W. Du, *Chem. Mater.*, 2015, **27**, 4586-4593.

34. J. J. Concepcion, J. W. Jurss, P. G. Hoertz and T. J. Meyer, *Angew. Chem. Int. Ed.*, 2009, **48**, 9473-9476.

35. F. Li, B. B. Zhang, X. N. Li, Y. Jiang, L. Chen, Y. Q. Li and L. C. Sun, *Angew. Chem. Int. Ed.*, 2011, **50**, 12276-12279.

36. M. R. Gao, W. C. Sheng, Z. B. Zhuang, Q. R. Fang, S. Gu, J. Jiang and Y. S. Yan, *J. Am. Chem. Soc.*, 2014, **136**, 7077-7084.

37. M. Gong, Y. G. Li, H. L. Wang, Y. Y. Liang, J. Z. Wu, J. G. Zhou, J. Wang, T. Regier, F. Wei and H. J. Dai, *J. Am. Chem. Soc.*, 2013, **135**, 8452-8455.

38. F. Yuksel, A. G. Gurek, C. Lebrun, V. Ahsen, *New J. Chem.* **2005**, *29*, 726-732.

39. J. J. Shao, J. J. Chang, C. Y. Chi, *Org. Biomol. Chem.* **2012**, *10*, 7045-7052.

Figures:

View Article Online
DOI: 10.1039/C7TA07978H

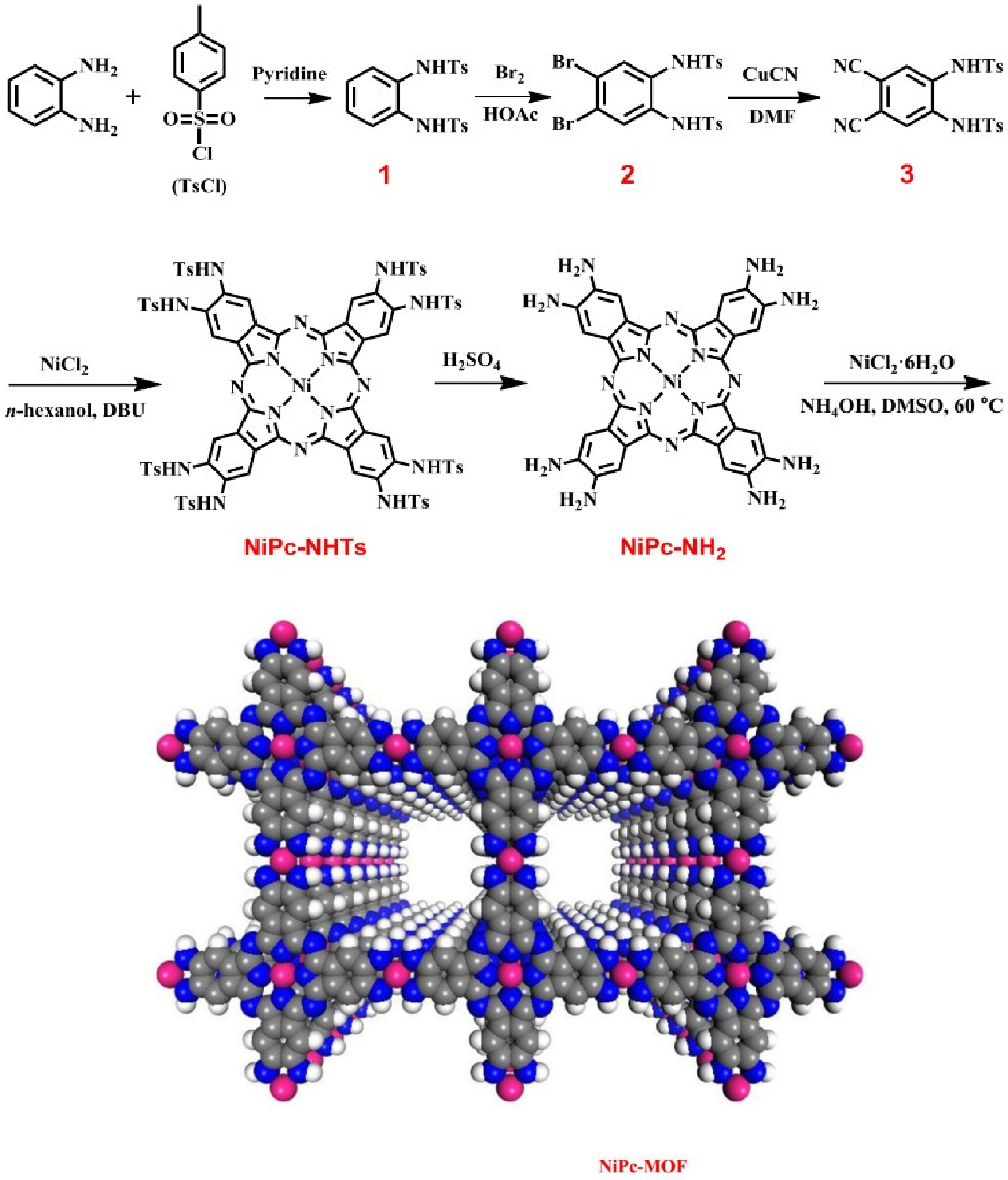

Figure 1. Chemical synthesis procedure of NiPc-MOF and its chemical structure.

View Article Online
DOI: 10.1039/C7TA07978H

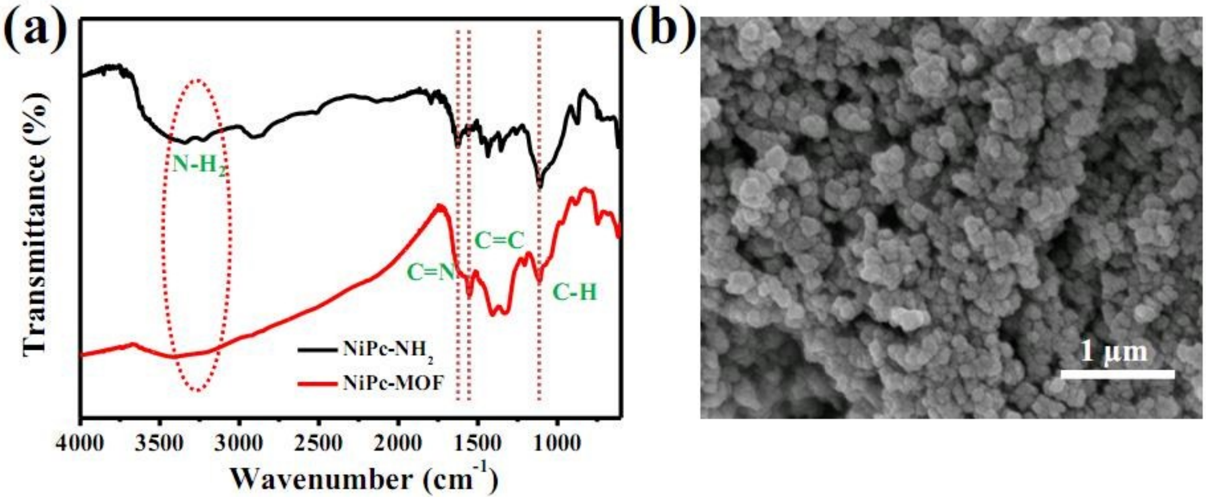

Figure 2. (a) FT-IR spectra of NiPc-MOF (red) and the NiPc-NH_2 monomers (black). (b) SEM image of bulk NiPc-MOF.

View Article Online
DOI: 10.1039/C7TA07978H

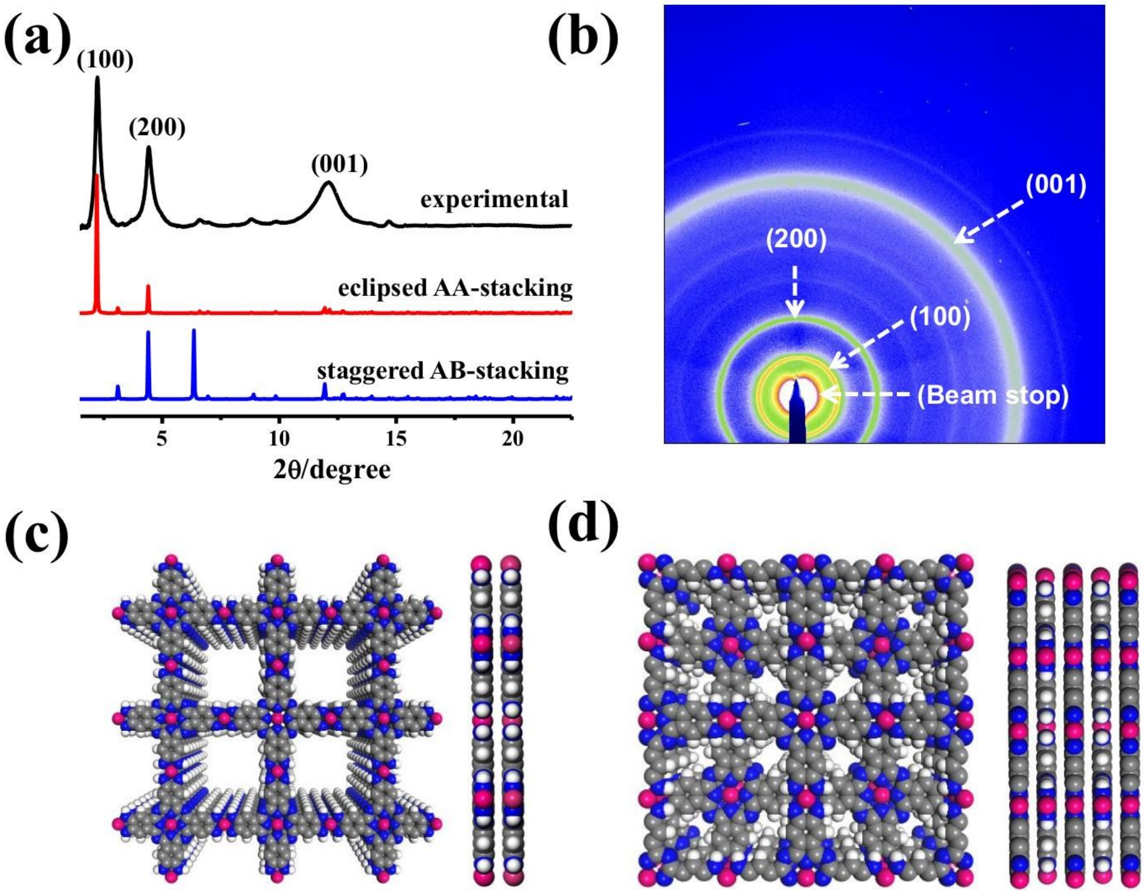

Figure 3. (a) Experimental XRD pattern (black) compared with simulated patterns (red and blue) using two different stacking arrangements for NiPc-MOF. (b) 2D synchrotron XRD pattern. (c) Eclipsed AA-stacking mode. (d) Staggered AB-stacking mode.

View Article Online
DOI: 10.1039/C7TA07978H

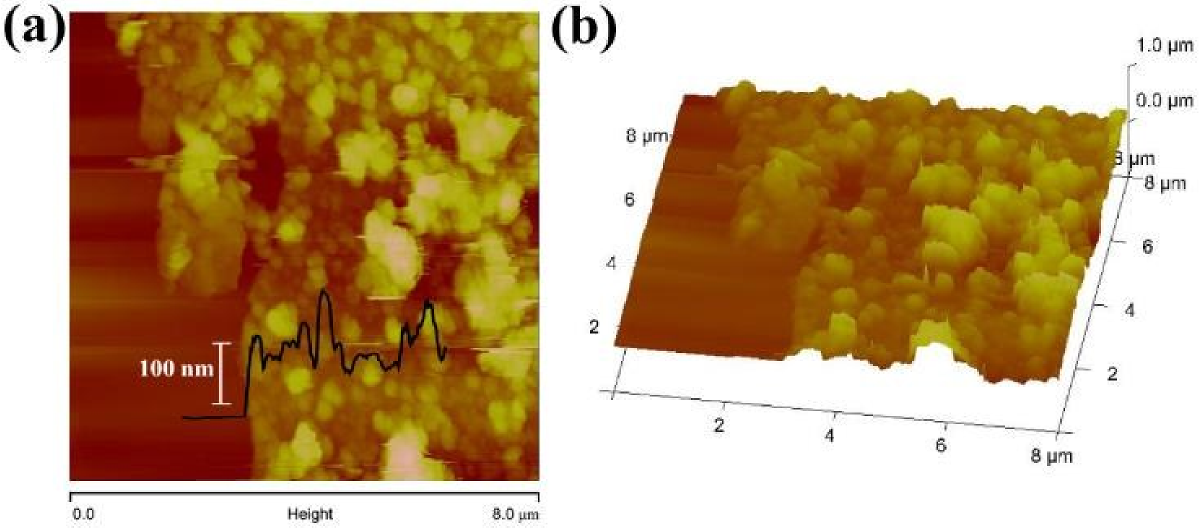

Figure 4. SPM height profile (black line) and corresponding morphology image of a typical NiPc-MOF film on quartz substrate. (b) 3D SPM image of the representative NiPc-MOF film.

View Article Online
DOI: 10.1039/C7TA07978H

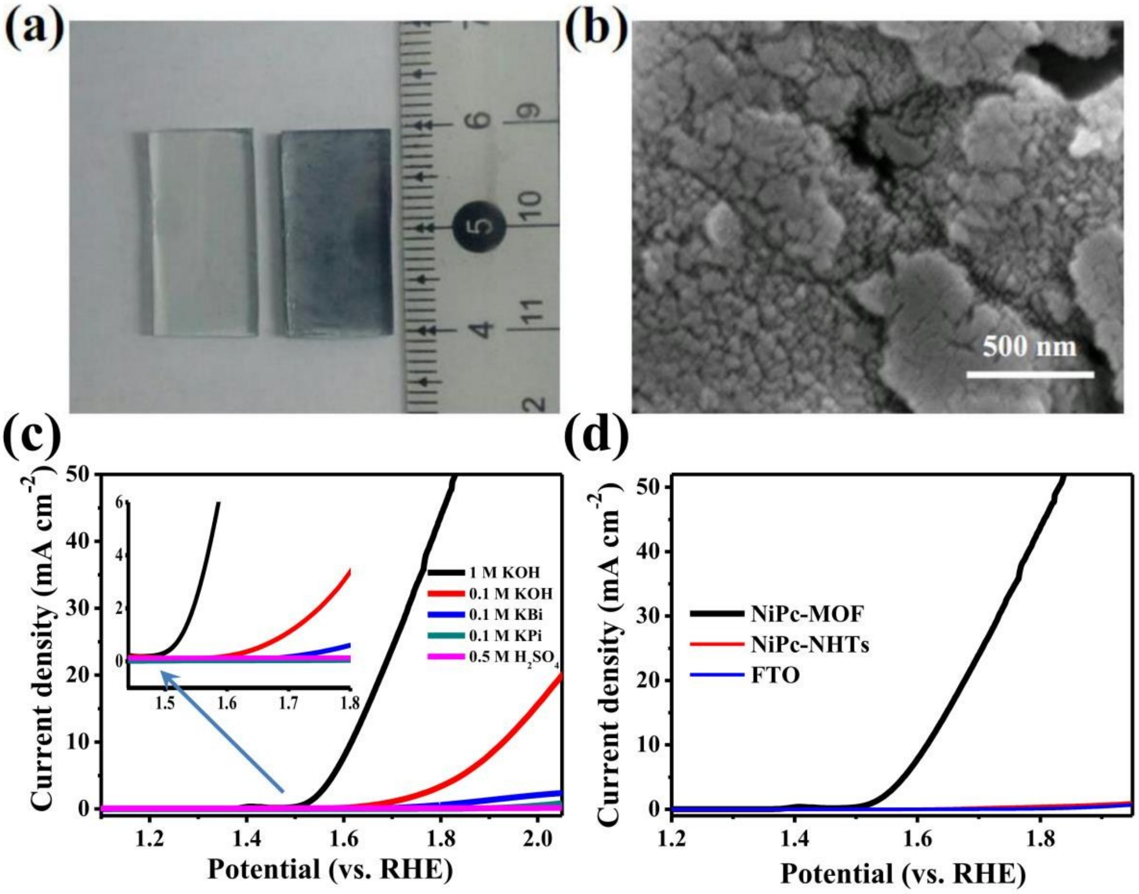

Figure 5. (a) Photograph of blank FTO (left) and NiPc-MOF modified FTO (right). (b) Top-down SEM image of NiPc-MOF film on FTO substrate. (c) pH-dependent LSV curves using NiPc-MOF as the OER catalyst. (d) LSV curves using NiPc-MOF, NiPc-NHTs monomers, and blank FTO as catalysts for OER. The scan rate was 10 mV/s.

View Article Online
DOI: 10.1039/C7TA07978H

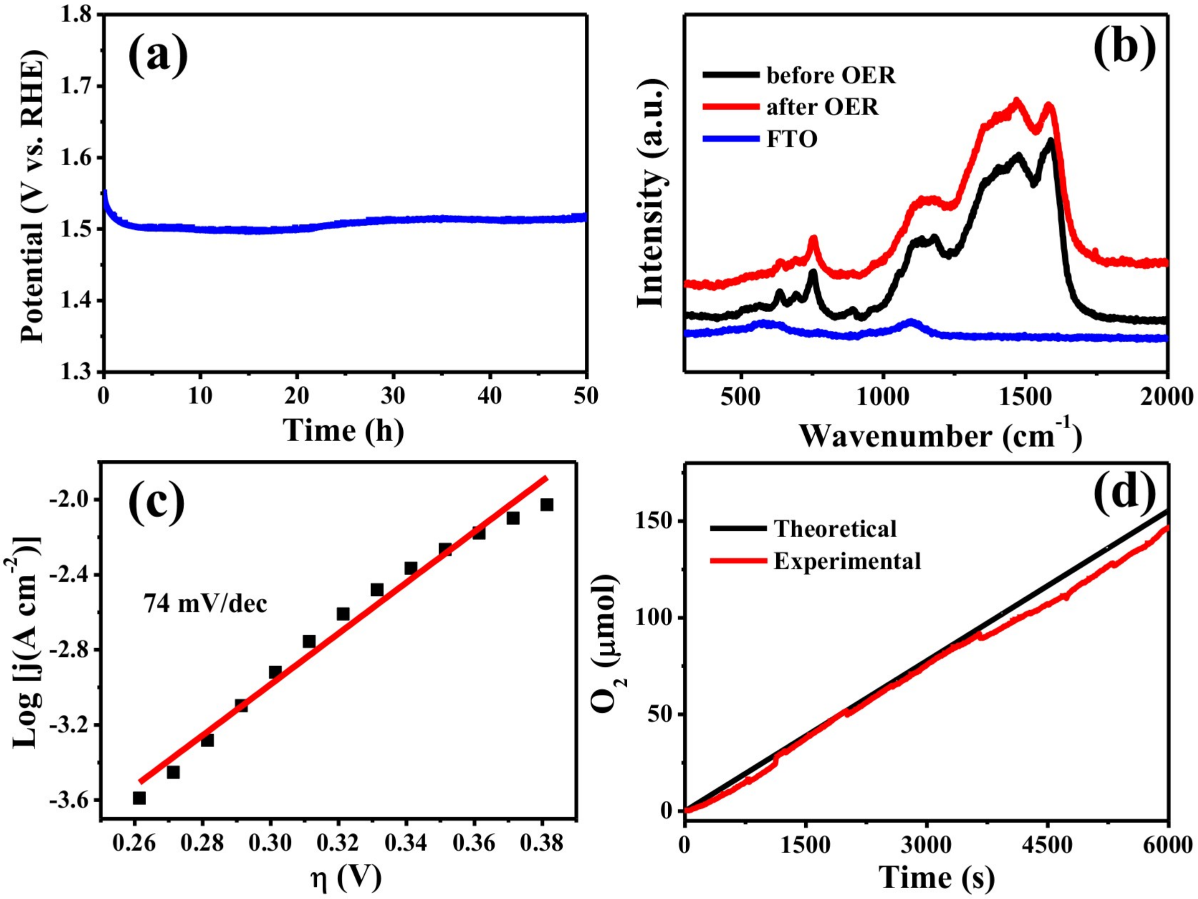

Figure 6. (a) Chronopotentiometry data for water oxidation under a fixed catalytic current density of 1.0 mA cm^{-2}. (b) Raman spectra of blank FTO (blue), freshly-prepared NiPc-MOF (black), and NiPc-MOF after long-term (> 5 hours) OER chronopotentiometry (red). (c) Tafel plot of NiPc-MOF. (d) Experimental oxygen production matched well with the theoretical value. The bulk electrolysis was performed under a fixed current density of 10 mA cm^{-2}.

View Article Online
DOI: 10.1039/C7TA07978H

TOC Figure